Agricultural Systems 228 (2025) 104367

Contents lists available at ScienceDirect

Agricultural Systems

journal homepage: www.elsevier.com/locate/agsy

Research Paper

Integrating crop models and machine learning for projecting climate change impacts on crops in data-limited environments

Seyyedmajid Alimagham [a,*], Marloes P. van Loon [a], Julian Ramirez-Villegas [a,b], Herman N.C. Berghuijs [a,c], Todd S. Rosenstock [d], Martin K. van Ittersum [a,e]

[a] Plant Production Systems Group, Wageningen University & Research, P.O. Box 430, 6700AK Wageningen, The Netherlands
[b] Bioversity International, Via di San Domenico 1, Rome, Italy
[c] Wageningen Environmental Research, Wageningen University & Research, P.O. Box 47, 6700 AA Wageningen, The Netherlands
[d] Bioversity International, Montpellier, France
[e] Department of Crop Production Ecology, Swedish University of Agricultural Sciences (SLU), P.O. Box 7043, Uppsala 75007, Sweden

HIGHLIGHTS

- A new approach is presented for large-scale applications using minimal data.
- Environmental conditions are taken into account in the training.
- The method was robust in 95 % of the cases for locations with available data.
- Potential uses: climate change impact and adaptation, breeding and policy decisions.

GRAPHICAL ABSTRACT

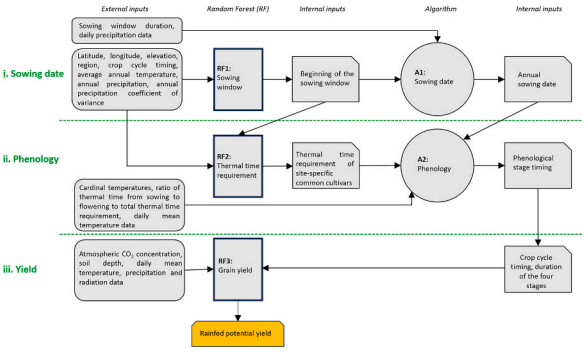

ARTICLE INFO

Editor: Leonard Rusinamhodzi

Keywords:
Adaptation
Phenology
Potential climate change impact
Sowing date

ABSTRACT

Context: Accurately projecting crop yields under climate change is essential for understanding potential impacts and planning of agricultural adaptation in sub-Saharan Africa (SSA). Crop growth models and machine learning (ML) are often used, but their effectiveness is limited by data availability, precision, and geographic coverage in SSA.

Objective: This study aimed to integrate ML with a process-based crop model to produce geographically continuous gridded crop yield projections while reducing uncertainties associated with standalone ML or crop growth models. As a case study, we implemented it to project the climate change impact on water-limited potential yield of maize across SSA.

Methods: We developed an integrated system that combines ML with eco-physiological processes to estimate sowing dates and thermal times, ensuring that crop phenology is accounted for, thus improving potential rainfed yield simulations under varying environmental conditions. Random Forest and crop model-based algorithms are integrated in three steps: (i) RF1, a Random Forest model integrated with a sowing algorithm, designed to estimate the sowing window and sowing date; (ii) RF2, a Random Forest model combined with a crop model

* Corresponding author.
E-mail address: m.alimagham@gmail.com (S. Alimagham).

https://doi.org/10.1016/j.agsy.2025.104367
Received 28 October 2024; Received in revised form 18 April 2025; Accepted 27 April 2025
Available online 9 May 2025

algorithm to estimate cumulative thermal time during the growing season, used to determine the timing of phenological stages; and (iii) RF3, another Random Forest model, trained based on eco-physiological principles applied in phases (i) and (ii), employed to simulate water-limited potential yield. The outcomes of the different steps of the framework under historical conditions were tested against reported data across SSA.

Results and conclusions: For maize and historical climatic conditions, the framework delivers yields which differ less than 20 % of those simulated with a crop model with high-quality inputs, in 95 % of the cases. Our approach thus shows value for generating crop yield projections in data-scarce regions under historical climate, and under future climatic conditions which already feature today somewhere in SSA and for which the framework has been trained.

Significance: Our approach can also be applied to other major food crops in SSA, under both current and climate change conditions. It allows testing the effect of adaptation of crop cultivars in terms of maturity group. Thus, it can be used for different crops and with far less data requirements compared to process-based crop models. It has the potential for significant applications in assessing climate change impacts, guiding adaptation strategies, and supporting crop breeding programmes and policymaking efforts in SSA.

1. Introduction

Projections indicate that climate change will impact crop yields in countries throughout sub-Saharan Africa (SSA) (Alimagham et al., 2024a; Jägermeyr et al., 2021), as their economies heavily depend on rainfed agricultural systems, which rely on adequate rainfall and temperature conditions to be productive (Kurukulasuriya et al., 2006; Mertz et al., 2009; Abrams, 2018). The potential impact of climate change on crop yields in SSA can be either positive or negative, depending on the region and the prevalent crop (Alimagham et al., 2024a). The ability to project crop yields under climate change conditions with sufficient precision is crucial for adaptation of agriculture across SSA.

The impact of climate change on crop yields in SSA using crop models is explored in a wide range of studies (e.g., Zhao et al., 2017; Hasegawa et al., 2022), but these studies either had to make generalized and coarse assumptions about e.g. crop calendars, soil conditions, and other management aspects (e.g., Jägermeyr et al., 2021; Stuch et al., 2021; Rosenzweig et al., 2014) or they are site-based studies that use high quality e.g. weather, management and soil data for the study sites which goes at the expense of geographic coverage (Asseng et al., 2015; Alimagham et al., 2024a). ML enables to accurately estimate crop yields in a variety of agro-ecological and management conditions including under climate change conditions (e.g., Li et al., 2023; Van Klompenburg et al., 2020). The drawbacks of this method are that it treats relationships in a system as a black box, making interpretability of the relationships difficult (Lischeid et al., 2022). Process-based models, like crop growth models, on the other hand are based on biophysical processes and are thus interpretable.

Combining ML with process-based models could enhance simulation capabilities across space and time, while also providing the necessary transparency in understanding the processes. Most studies that have attempted to combine crop models and ML for yield simulation have used crop model outputs as the input for training and employing ML algorithms (Li et al., 2023; Shahhosseini et al., 2021). Although this strategy improves the accuracy of ML in yield simulations, its applicability is limited to regions with sufficient data to run crop models. However, if ML models are trained and tested to mimic key components of mechanistic crop simulation models in data-rich regions using minimal input data, they can later be applied in data-scarce regions where limited data availability hinders the direct use of crop models. Achieving this, especially for yield projections under climate change scenarios, requires ML to adequately capture key dynamic eco-physiological processes and cropping system principles.

Crop growth and development rates, and resulting yields can vary over time at a specific location due to changes in environmental conditions caused by climate change (Guo et al., 2021). If phenology projections are inaccurate, yield simulations will also be unreliable, as growth processes would occur at different times and under conditions that do not reflect actual circumstances. At least two key inputs are needed to ensure phenology projections are robust, (1) sowing dates; (2) thermal time requirement of crops (Fatima et al., 2020; Zimmermann et al., 2017). These parameters vary greatly across SSA. For instance, the start of the cropping season is determined by the onset of the rainfall across SSA, which exhibits significant variability across different sites, years, even across relatively small geographic distances (Agossou and Kang, 2020). Therefore, in order to determine the phenology timing of crops in different regions of SSA, it is imperative to have a comprehensive and site-specific dataset, which is currently lacking for SSA. Instead, fixed-time data, such as annual, seasonal, or monthly data, are commonly used for training ML algorithms (Aramburu-Merlos et al., 2024; Lischeid et al., 2022. Using ML algorithms based on crop growing season data can enhance the accuracy of simulations.

Actual farm yields in SSA remain substantially below their potential, primarily due to nutrient limitations (Ten Berge et al., 2019; Sánchez, 2010), and must increase markedly to meet future food demand (Van Ittersum et al., 2016; Sánchez, 2010). Water-limited yield potentials, including projections under climate change, provide the benchmark for identifying yield gaps and guiding research and development priorities (Van Oort, 2018). They also offer a basis for estimating the additional nutrient inputs required to achieve target yields necessary for future food security (Ten Berge et al., 2019).

The Global Yield Gap Atlas (GYGA, www.yieldgap.org) delivers robust (potential) yield projections by using local data (soil, management, weather) from key production sites as input for crop growth models in combination with a bottom-up spatial framework for upscaling to larger spatial scales (Van Wart et al., 2013). Despite the use of the upscaling procedure, the spatial coverage is still a limitation especially in data-scarce regions like SSA (Rattalino Edreira et al., 2021; Aramburu-Merlos et al., 2024). A recent study used the GYGA data to assess climate change impacts on key rainfed cereal crops (maize, wheat, sorghum, millet) in the region (Alimagham et al., 2024a, 2024b). It encompasses key production sites across ten countries, rather than the entire SSA region. Here, we leverage this robust dataset for training ML techniques and extrapolating the results to the entire SSA using a stepwise framework. This framework integrates key mechanisms captured with a crop model (timing sowing, crop phenology, and grain yield) to achieve the best possible accuracy in projecting climate change impacts using ML. The advantage of this stepwise approach is that it builds mechanistic detail into our framework while capitalising on the advantages of ML models in terms of simpler structure, fewer input requirements and easier replicability.

The aim of this study was to integrate ML with a process-based crop model, grounded in eco-physiological principles, to generate spatially continuous, gridded projections of potential rainfed yields in SSA. This integration focused on using high-quality data from existing, data-rich sites to train ML. It also ensured that the trained model could be applied to data-limited areas, without needing the extensive input datasets usually required by process-based crop models. Additionally, the framework allows for the use of the trained ML under climate change conditions. As case study, we implemented it to project the climate

change impact on potential maize yields across SSA. The proposed framework utilizes point-based data (from GYGA, Alimagham et al., 2024b) for ML model training, while also minimising the required input data and complexity of the modeling framework under current and future climate conditions. We tested the modeling framework within- and out-of-sample to demonstrate its applicability for climate change studies.

2. Method

The framework integrates Random Forest (RF) and crop model-based algorithms in three steps: (i) RF1, a Random Forest model integrated with a sowing algorithm named A1, designed to estimate the sowing window and sowing date; (ii) RF2, a Random Forest model combined with a crop model algorithm named A2 to estimate cumulative thermal time during the growing season, used to determine the timing of phenological stages; and (iii) RF3, another Random Forest model, developed based on eco-physiological principles, employed to simulate water-limited potential yield. The combination of the crop modeling and ML was structured as follows (Fig. 1): First, the RF1, in conjunction with a sowing date algorithm, determined region-specific sowing dates. Next, using the RF2, the cumulative thermal time required from sowing to harvest was estimated for each region. This estimation relied on the daily thermal time calculation algorithm from the crop model, along with the outputs from the RF1 and RF2. At this stage, the length of the growth period was simulated, enabling the division of the growing season into four distinct periods. Finally, the RF3 utilized this data to simulate crop yield by incorporating environmental data for each growth stage. Training the RF3 model with data from different growth stages as simulated through steps i and ii is crucial because sub-optimal conditions in one growth stage, such as water stress or high temperature, could affect crop growth in subsequent stages. The combination of these models thus builds mechanistic details into our framework while capitalizing on the advantages of RF models in terms of simpler structure, fewer input requirements, and easier replicability.

2.1. Input data

Two groups of data are required for the framework, namely internal inputs and external inputs (Fig. 1). External data refers to e.g. daily weather data and soil depth (Fig. 1), while internal inputs refer to generated outputs of the algorithms or RFs which are then used as inputs for the subsequent crop model algorithm or RF (Fig. 1).

Training and testing of each of the three steps within the framework are done using data as presented by Alimagham et al. (2024b). This study employed the simulated rainfed potential yields across 105 representative maize production sites from ten sub-Saharan countries, namely Burkina Faso, Ghana, Mali, Niger, Nigeria, Ethiopia, Kenya, Tanzania, Uganda, and Zambia (Fig. S1). The representative maize production sites were chosen to represent production but also to ensure that weather data is of the highest quality possible. For each site, a representative weather station (RWS) is available in this dataset. The sites were selected and the RWS data derived using the protocol established by the Global Yield Gap Atlas (Grassini et al., 2015; van Bussel et al., 2015). The GYGA protocol seeks to achieve 50 % coverage of national harvested crop area within buffer zones of the RWS, ensuring the inclusion of crucial climate zones (van Bussel et al., 2015). The climate zone map created by the GYGA was used for this purpose (Van Wart et al., 2013, and available online at https://www.yieldgap.org/web/guest/climate-zones). This map identifies climate zones using three indices: (i) cumulative annual growing days based on a base temperature of 0 °C, (ii) an annual aridity index, defined as the ratio of mean

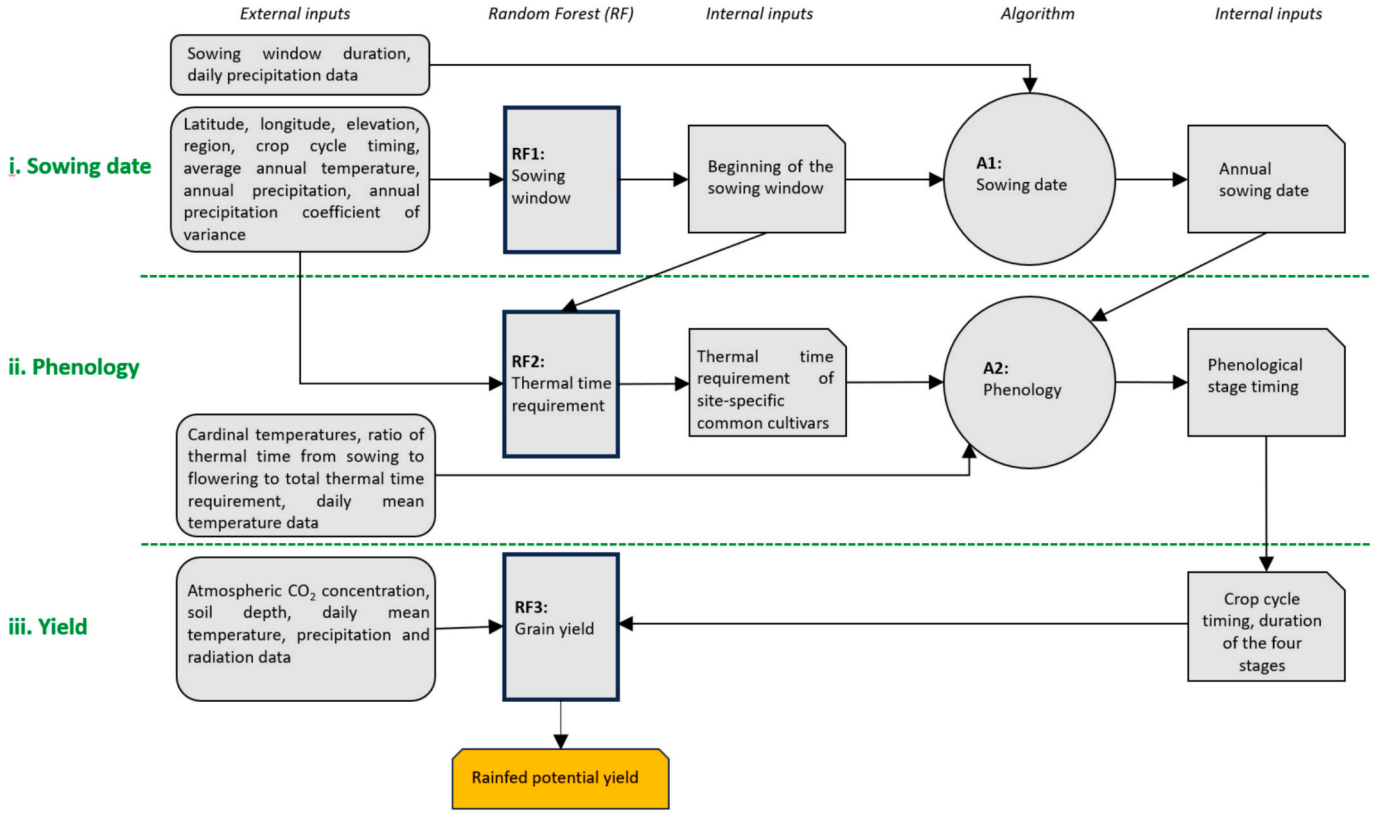

Fig. 1. Flowchart of the designated framework showing the connections between the three random forest (RF) components and two crop model algorithms (A) in our approach. The framework consists of three steps: i) estimation of annual sowing dates, ii) simulation of phenological stage timings, iii) simulation of rainfed potential yield. Green dashed lines indicate the steps within the framework. See Table 1 for sources of datasets included in the framework. (For interpretation of the references to colour in this figure legend, the reader is referred to the web version of this article.)

annual precipitation to mean annual potential evapotranspiration, and (iii) temperature seasonality, calculated as the standard deviation of the 12 monthly mean temperatures. Since temperature seasonality was largely uniform across SSA, except in a small part of South Africa, we represented the climate zones using only the first two indices. To enhance the understanding of the thermal time index of each climate zone, we converted it to the mean annual temperature by dividing it by 365 (the number of days in a year). Furthermore, the simulation results indicated that zones with an aridity index greater than 30 % experienced no water stress impact on potential rainfed yields of maize (data not shown), leading us to classify these areas as wet climates. Moreover, climate zones with an aridity index below 30 % were designated as dry areas. Crop area data from the Spatial Allocation Model map version 2020 (SPAM2020; International Food Policy Research Institute (IFPRI), 2024) was used to calculate the coverage of maize land within each climate zone.

For each site, the GYGA dataset provided RWS coordinates along with crop management (sowing windows), and crop phenology data (flowering and harvesting time) under historical conditions, and simulated rainfed potential maize yields under current and future conditions. To train ML models, we also employed daily bias-corrected weather data for two Shared Socioeconomic Pathways (SSPs; SSP3–7.0 and SSP5–8.5), obtained from five different General Circulation Models (GCMs; GFDL, IPSL, MPI, MRI, UKESM) from the Coupled Model Intercomparison Project Phase 6 (CMIP6) model ensemble (Alimagham et al., 2024b). We chose SSP5–8.5 as it shows the largest departures from historical climate and hence would constitute suitable scenarios for evaluating our modeling framework. In addition, we used SSP3–7.0 because it is the closest to the world's current emissions trajectory, and thus a suitable indicator of climate change impacts especially by 2050s. The time horizons considered were the historical period (1995–2014), as well as 2030 (2020–2039) and 2050 (2040–2059) (Alimagham et al., 2024b).

The training dataset for weather data and for potential rainfed yield at RF3 consisted of 20 % of the total data for only climate change scenario SSP5–8.5, leading to a training dataset consisting of ca. 54,000 simulated data points. It includes all possible combinations of GCMs, stations, soil types, and cropping season timing, covering different time horizons. For testing the model, the remaining 80 % of data for climate change scenario SSP5–8.5 (ca. 216,000 data points) and the full dataset for climate change scenario SSP3–7.0 (270,000 data points) were used (Alimagham et al., 2024b). Hereafter, we first present each of the steps within the framework and its application to the RWS data for representative production areas in the ten countries (Sections 2.2–2.4), then further details are provided on how the framework can be applied to the virtual weather stations (VWS) for all maize land across the entire SSA (Section 2.5), and finally, we explain how it is tested against the Evidence for Resilient Agriculture (ERA) version 1.01 dataset, which includes field experiments conducted across SSA (Rosenstock et al., 2024) (Section 2.6).

2.2. Step i, estimation of annual sowing dates

2.2.1. The random Forest model to determine the start of the sowing window (RF1)

The first Random Forest model is used to estimate the beginning of the sowing window at each location across SSA, hereafter called RF1. In SSA, the growing season begins with the onset of rainfall. There is considerable spatial variation in the onset of rainfall in SSA, which is strongly influenced by latitude (Obarein and Amanambu, 2019). Altitude is another factor which can affect the onset of rainfall in SSA (Ngetich et al., 2014). As a result, we chose the following independent variables for RF1: coordinate, elevation, region (determined by its proximity to the equator or its location in the northern/southern hemisphere), and crop season timing within RWSs (in the northern hemisphere, the value is 1 which shows the season starts after April; in the southern hemisphere, it is 2 which shows the season starts after October; for equatorial regions, it encompasses both 1 and 2 because of double cropping over the year in this area), average annual temperature, annual precipitation, and annual precipitation coefficient of variance. The dependent variable was the common beginning of the sowing window within buffers around RWSs. RF1's output is the average start and end of the sowing window, that is based on the mean climate and geographic location of each buffer area. The GYGA dataset used by Alimagham et al. (2024b) from ten countries provides all necessary data to train and test the performance of the RF1 (Table 1). The data was randomly split into a training set (70 % of the data) and a test set (30 % of the data).

Table 1
The source of datasets employed to train and apply the algorithms.

Data	Source of the data	
	For training	For SSA-wide simulations
Latitude	Alimagham et al. (2024b)	Location of VWS*
Longitude	Alimagham et al. (2024b)	Location of VWS
Elevation	https://www.freemaptools.com/elevation-finder.htm	https://www.freemaptools.com/elevation-finder.htm
Region	**	**
Daily rainfall data	Alimagham et al. (2024b)	See Section 2.5
Daily temperature data	Alimagham et al. (2024b)	See Section 2.5
Daily radiation data	Alimagham et al. (2024b)	See Section 2.5
Crop season timing	GYGA dataset$	***
Beginning of the sowing window	GYGA dataset	**Calculated by RF1**
Sowing window duration	GYGA dataset	Adding 60 days to beginning of the sowing window
Sowing date algorithm #	Van Loon et al. (2018)	**Calculated by A1**
Thermal time requirement from sowing to maturity	GYGA dataset	**Calculated by RF2**
Cardinal temperatures of maize	WOFOST ##	WOFOST ##
Ratio between thermal time from sowing to flowering and total thermal time requirement	GYGA dataset	GYGA dataset
Timing of the four growing stages ###	Alimagham et al. (2024b)	**Calculated by A2**
The duration of each growth stage	WOFOST ##	See Section 2.3
CO_2 concentration	CMIP6 @	CMIP6 @
Soil depth	AfSIS (Leenaars et al., 2018)	AfSIS (Leenaars et al., 2018)
Rainfed potential yield	Alimagham et al. (2024b)	**Calculated by RF3**

A consecutive 7 days within the sowing window with at least 20 mm rainfall.
https://github.com/ajwdewit/WOFOST_crop_parameters
Stage I, early vegetative growth stage; Stage II, late vegetative growth stage; Stage III, early reproductive growth stage; Stage IV, late reproductive growth stage.
$ Global Yield Gap Atlas (https://www.yieldgap.org/web/guest/climate-zones)
@ The data for climate change scenarios SSP3–7.0 and SSP5–8.5 were downloaded from ISIMIP3b repository (Büchner and Reyer, 2022) the CMIP6 data repository.
* Virtual weather station.
** Regions with a latitude greater than 5° are classified as part of the northern hemisphere, while those between −5° and 5° are regarded as equatorial regions. Latitudes less than −5° are categorized as the southern hemisphere.
*** In the northern hemisphere, the value is 1; in the southern hemisphere, it is 2; for equatorial regions, it encompasses both 1 and 2 because of the double cropping over the year system in this area over the year.

2.2.2. The crop model algorithm to determine sowing dates (A1)

The algorithm A1 estimates year-specific and site-specific sowing dates using the RF1 model output, the timing of the start of the sowing window, together with a sowing window duration of 60 days. The algorithm calculates the cumulative rainfall for seven consecutive days over the sowing window. The last day of this period, when cumulative rainfall exceeds 20 mm, is considered the sowing date. If there is not at least 20 mm rainfall in seven convective days within the sowing window, the last day of the sowing window is assumed to be the sowing date (Van Loon et al., 2018). This algorithm provides an optimal sowing date across SSA (Wolf et al., 2015).

2.3. Step ii, simulation of phenological stage timings

2.3.1. The random Forest model to assess the thermal time requirement (RF2)

The second Random Forest model, RF2, used the GYGA dataset for RWS for training to calculate the required total thermal time from sowing to maturity for maize at each site. The GYGA data used by Alimagham et al. (2024b) was randomly split into a training set (70 % of the data) and a test set (30 % of the data). The independent variables consist of all the independent variables employed in RF1, along with the initiation of the sowing window (Fig. 1), and the dependent variable is the total thermal time (from sowing to maturity) of common cultivars in terms of phenology in each RWS under historical climate conditions. The thermal time requirements of cultivars commonly grown in each RWS are determined on the GYGA dataset, as specified by local experts.

2.3.2. The crop model algorithm for phenology (A2)

The algorithm for phenology named A2 simulates the timing of four stages throughout the growing season, namely: Stage I, early vegetative growth stage; Stage II, late vegetative growth stage; Stage III, early reproductive growth stage; Stage IV, late reproductive growth stage. This segmentation allows for the capture of the eco-physiological responses of crops during each stage (Table 2; Table S1). We divide the growing season in these different stages as stresses (like water stress) have a different impact on each stage. For example, although water stress across the growing season can decrease grain yield, water stress during grain filling (i.e. Stages III and IV) has normally the largest negative impact on the grain yield (Cakir, 2004). The eco-physiological differences between the different stages are presented in Table 2 and the impact of different variables on capturing physiological responses in training algorithms is presented in Table S1.

For this purpose, the period from sowing to flowering is divided into two equal periods in terms of thermal time requirement (Stage I, Stage II). The same is done for the period from flowering to maturity (Stage III, Stage IV). The ratio of cumulative thermal time from sowing to flowering to total thermal time requirement from sowing to maturity was calculated using GYGA's observed data, resulting in an average value of 0.55 with standard deviation equal to 0.04. Note, that this parameter is adjustable in our approach, enabling simulations with different values in different runs.

The annual sowing date and site-specific thermal time of cultivars from sowing to maturity are then used by A2 to estimate the timing of the four stages over the growing season. For this purpose, the phenology module within the WOFOST model for maize was used (De Wit et al., 2019). In this module, the development rate is linearly related with average daily temperature if the daily mean temperature is larger than the base temperature but smaller than the optimum temperature. If the daily mean temperature is larger than the optimum temperature, the development rate remains constant (Eq. 1). If simulation results from another crop model are to be used in training, it is advisable to use the corresponding phenology model.

$$\text{If } t \le t_b \qquad DTT = 0 \tag{1}$$

$$\text{If } t_b < t < t_{op} \qquad DTT = t - t_b$$

$$\text{If } t \ge t_{op} \qquad DTT = t_{op} - t_b$$

t: daily mean temperature (°C).
t_b: base temperature for maize growth which was set at 10 °C.
t_{op}: optimum temperature for maize growth which was set at 30 °C.
DTT: daily thermal time caught by maize (degree day).

Since the beginning of the sowing window is one of the inputs for the RF2 model (Fig. 1; Table 1) and the output of the RF1 model, we can estimate the thermal time requirements of common maize cultivars across various locations in SSA by integrating the RF1 and RF2 models (Fig. 1; Table 1). It is imperative to emphasize that RF2 solely calculates thermal time for historical conditions, with the aim of identifying site-specific common cultivars based on their thermal time requirements. The thermal time requirements of cultivars employed for future climate conditions (time horizons 2030 and 2050) will remain unchanged. Although the thermal time requirements remain constant, the timing of the four stages can be altered because of increasing temperatures caused by the changing climates in 2030 and 2050 compared to historical conditions. Additionally, the system has been designed in a way that allows for the adjustment of thermal time values calculated by the RF2. This enables the evaluation of new cultivars in terms of early or late maturity groups in each site across SSA under historical and future climate conditions.

Table 2
Eco-physiological differences across the four growth stages of maize, i.e., Stage I, early vegetative growth stage; Stage II, late vegetative growth stage; Stage III, early reproductive growth stage; Stage IV, late reproductive growth stage.

Eco-physiological feature	Stage I	Stage II	Stage III	Stage IV
Canopy ground cover	open	close	close	reopening*
Transpiration/ evapotranspiration ratio	low	high	high	low*
Water use efficiency**	low	high	high	low
Main sink	vegetative organs	vegetative organs	grain	grain

* Depending on leaf senescence rate (See Fig. S2).
** Ratio between dry matter and evapotranspiration (See Fig. S2).

2.4. Step iii, simulating rainfed potential yield

2.4.1. The random Forest model to simulate rainfed potential yield (RF3)

The dependent variable in the RF3 model is the rainfed potential yield. The independent variables include average temperature, cumulative rainfall, and cumulative radiation during each of the four stages, duration of the stages, crop season timing (see section 2.2.1), atmospheric CO_2 concentration, soil depth (Fig. 1, Table 1). Despite variation in cultivars, temperatures, and the influence of climate change on phenological stages across SSA, the implementation of the thermal time requirement model (RF2) allows a consistent identification of developmental stages during the maize growing season. The inclusion of soil depth as an independent variable is based on the important relationship between soil depth, available water for crop growth and maize yield at a given precipitation (Calviño et al., 2003). The dominant soil types in terms of maximum rootable depth within each buffer zones of 100 km around a RWS location (clipped by climate zones – see van Bussel et al., 2015) were determined using AfSIS data (Leenaars et al., 2018); Up to three dominant soil depths were selected until achieving 50 % area coverage per buffer zone. All soil units with over 10 % area coverage of maize lands were used for buffers that did not meet the 50 % coverage requirement.

Despite variation in temperature, similar growing season durations can be observed in different regions of SSA due to the use of different maturity group cultivars across regions in this study. Consequently,

different regions can experience varying temperature and cumulative radiation levels during the growing season, despite having the same growing season duration. In areas that experience lower temperatures, specifically in Eastern and Southern Africa, there is an expected elongation of the period in which leaves stay green, while leaves will have shorter stay green periods due leaf senescence under rising temperatures (Hu et al., 2023). The inclusion of the duration of the four stages as independent variables in the RF3 model (Fig. 1) aims to capture the influence of stress duration (water stress or high temperature) in each stage (Hu et al., 2023; Ge et al., 2012). The important aspects of water and/or temperature stress include intensity of stress, timing of stress, and duration of stress (Riedesel et al., 2023; Cavus et al., 2023). The intensity can be captured by rainfall data combined with radiation, temperature, and soil depth, all of which are included in the training of the RF3. The timing can be captured in RF3, because we divided the growing season into four different stages, and the environmental data for each stage is used separately in training RF3. Finally, the duration of the stress can be captured by the duration of each growth stage, which is also included in the training of RF3.

2.5. Data for geographically continuous and SSA-wide rainfed potential yield projections

To allow for geographically continuous and SSA wide rainfed potential yield projections we followed the GYGA protocol for creating and scaling yield projections (van Bussel et al., 2015). This implies that we first created a continent-wide network of 1500 VWSs, with a buffer area of 100 km radius around each VWS. The buffers were clipped to align with the surrounding climate zones, ensuring uniform climate coverage for each buffer zone while preventing overlap with other buffer zones. The GYGA climate zone map was employed for this purpose (Van Wart et al., 2013, and available online at https://www.yieldgap.org/web/guest/climate-zones). Buffer areas with a maize harvested area of less than one hectare are excluded, using the SPAM2020 map (International Food Policy Research Institute (IFPRI), 2024) (Fig. S3), resulting in a total of 1300 VWS covering the entirety of SSA (Fig. S3).

Daily weather data at each VWS, including rainfall, minimum and maximum temperatures, and solar radiation, were required for historical (1995–2014) and future (2020–2039 and 2040–2059) periods. Historical rainfall data were taken from the Climate Hazards Infra-Red Precipitation with Stations (CHIRPS, Funk et al., 2015), historical temperature data were gathered from the Climate Hazards Infra-Red Temperature with Stations (CHIRTS) (Funk et al., 2019), and solar radiation was derived from the agriculture-focused version of the European Center for Medium-range Weather Forecasts (ECMWF) Reanalysis version 5 (AgERA5; Boogaard and van der Grijn, 2020). For each VWS, we extracted daily values for each of the variables from the corresponding dataset. To create the future projections, we used bias-corrected data from General Circulation Models from the Coupled Model Intercomparison Project Phase 6 (CMIP6) model ensemble under two climate change scenarios (SSPs; SSP3–7.0 and SSP5–8.5) using the 'delta' method as described by Navarro-Racines et al. (2020).

2.6. Framework evaluation

The outcomes of the different steps of the framework under historical conditions were also tested against the Evidence for Resilient Agriculture (ERA) version 1.01 dataset, which included field experiments conducted across SSA (Rosenstock et al., 2024). ERA v1.01 is a large meta-analysis of 2011 agronomic experiments in Africa covering the period 1934–2018. The dataset encompasses a total of 112,859 individual observations covering the effect of 363 agronomic, livestock, or tree management techniques and their combinations on more than 75 metrics of productivity, resilience, and greenhouse gases.

Step i outcomes on sowing dates was evaluated using a total of 422 data points on maize sowing date from the ERA dataset. Step ii outcomes on durations (sowing-maturity) was evaluated with measured growing season durations (sowing-harvest) using a total of 454 data points from the ERA dataset. As the ERA dataset lacked information regarding the thermal time requirement of cultivars. Additionally, Step ii was evaluated against data collected by Abate et al. (2017) on dominant maize cultivars in various countries. The information on dominant maize cultivars was combined with information on the length of the growing season for these cultivars in each country which was gathered from seed companies and research institutes (Table S2). The dominant regions per country were determined by utilizing simulated results from buffer zones that covered 75 % of the total maize area in each country. This restriction was accounted for due to the fact that the dominant cultivars identified by Abate et al. (2017) did not cover all cropland in the countries. Note, that the reported lengths of the growing season for the cultivars offered by seed companies and research institutes are typically adapted to the primary regions within each country. In addition, it should be noted that the reported growing season durations for the dominant cultivars are referring to the period between sowing to maturity unlike the ERA dataset which is from sowing to harvest (Table S2).

Step iii was evaluated by comparing the simulated rainfed potential yields against observed yields from experiments in the ERA dataset. The ERA dataset underwent a multi-stage filtering method, retaining only the experiments with the highest yields within each buffer zone (Table 3).

2.7. Sensitivity analysis

In addition to evaluating our method's outputs using different datasets (Section 2.6), we conducted a sensitivity analysis. We systematically categorised the simulated rainfed potential yields from Alimagham et al. (2024b) for the RWSs, considering factors such as climate change scenarios, GCMs, and soil depth. We compared the cumulative estimated rainfed potential yield distributions from RF3 with those estimated by WOFOST under various climate change scenarios and time horizons for each category. Furthermore, we calculated the annual absolute relative change in yields simulated by the RF3 model in comparison to the simulated results generated by the crop model. The correlation between the calculated absolute relative values and cumulative rainfall or average temperature was assessed across the four growing stages.

2.8. Software and packages

A Random Forest model is an ensemble learning method that combines multiple decision trees to improve accuracy and reduce overfitting (Breiman, 2001). It works by training several decision trees on different subsets of the data and then aggregating their simulations. The model creates multiple decision trees by randomly sampling the training data

Table 3
The steps for filtering ERA data in order to identify experiments with highest yields.

Step	Filtering based	Number of (remaining) data entries
0	All ERA data: no filter	116,243
1	Crop: keep data only for maize with yield data	23,161
2	Rainfed system: keep data only for rainfed conditions	21,076
3	Buffer zone: keep only 15 % of the highest yields within each buffer zone	2112
4	Study: keep only 50 % of the highest yields for each study within each buffer zone*	1200
5	Removing duplicated values for each study within each buffer zone	607

* This filter was applied to retain only the treatments from similar experiments that produced the largest yields.

with replacement (Breiman, 1996). The final simulation is the average of individual tree outputs (Breiman, 2001). Previous studies have demonstrated that Random Forest can accurately simulate crop yields (Van Klompenburg et al., 2020; Jeong et al., 2016). The number of trees (ntree) was set to 500, and number of variables randomly sampled as candidates at each split (Mtry) was calculated by dividing the total number of features by 3 for each Random Forest model (RF1, RF2, RF3). Training and testing of the ML algorithms were conducted using the randomForest package in R language (Breiman, 2001). The caTools package was used for splitting the data into the train and test sets (https://cran.r-project.org/web/packages/caTools/index.html). The entire framework (Fig. 1) was coded in a comprehensive R script using the tidyverse package (https://cran.r-project.o rg/web/packages/tidyverse/index.html).

3. Results

3.1. The performance of the algorithms

3.1.1. RF1 and the A1 algorithm for sowing date

The nRMSE for estimating the beginning of the sowing window using the GYGA dataset for testing the RF1 model was 17.1 % (Fig. 2a; Table 4). The combination of the RF1 model and the A1 algorithm effectively estimates sowing dates for each year across SSA (Fig. 2b). In addition, results demonstrate that the efficacy of combining the RF1 model and the A1 algorithm for determining site- and year-specific sowing dates for the various countries across SSA (Fig. 2b). The algorithms provide accurate estimations of the sowing dates throughout SSA, despite the enormous variation in sowing dates across Eastern and Southern Africa (Fig. 2b). The simulated sowing date in West Africa occurs slightly earlier than the ERA sowing data, with the fourth quartile of the simulated data overlapping the first quartile of the ERA data in the majority of countries in West Africa (Fig. 2b). This overlap indicates that the sowing window is estimated with reasonable accuracy; however, the algorithm used to determine the sowing date within the window tends to calculate the sowing dates somewhat earlier than the ERA data.

3.1.2. RF2 and the A2 algorithm for phenology

The test dataset of the GYGA data demonstrated that the RF2 model has a good performance in estimating the total thermal time requirement from sowing to maturity of maize (nRMSE = 10.3 %; Fig. 3a, Table 4). Note that the thermal time of maize cultivars at the GYGA RWS stations ranged from 900 to 1900 degree days, which is well captured by the RF2 model, with good simulations of site-specific cultivars using environmental inputs across SSA (Fig. 3a; Table 4).

A systematic bias exists in the comparison of simulated growing season durations from sowing to maturity with the ERA data. In general, the simulated values are lower than those reported in the ERA dataset (Fig. 3b). However, this bias is not present when comparing the simulated values in the dominant regions in terms of area for the crop with the reported duration of the growing season for the primary cultivars provided by seed companies and research institutes in each country (Fig. 3c).

3.1.3. RF3 and the entire system

In order to evaluate the performance of all algorithms jointly (RF1

Table 4
Statistical metrics for evaluating the accuracy of the algorithms using training or testing datasets from GYGA RWSs. For the meaning of abbreviations of the algorithms see Fig. 1.

Algorithm	Training			Testing		
	R2	RMSE*	nRMSE (%)	R2	RMSE*	nRMSE (%)
RF1	0.97	0.5	9.8	0.89	1.0	17.1
RF2	0.91	92.1	5.9	0.56	162.3	10.3
RF3-SSP5–8.5-2005	0.97	0.7	8.0	0.89	1.3	15.6
RF3-SSP5–8.5-2030	0.98	0.5	6.7	0.89	1.2	14.6
RF3-SSP5–8.5-2050	0.98	0.5	7.1	0.87	1.2	16.2
RF3-SSP3–7.0-2005**	–	–	–	0.91	1.2	14.4
RF3-SSP3–7.0-2030**	–	–	–	0.87	1.3	16.0
RF3-SSP3–7.0-2050**	–	–	–	0.84	1.3	18.0

* The unit of RMSE for the RF1 is specified as "month" while for RF2 it is "growing degree day" and for RF3 it is "ton/ha".
** These data were solely employed for the purpose of testing the algorithm trained with the SSP5–8.5 data.

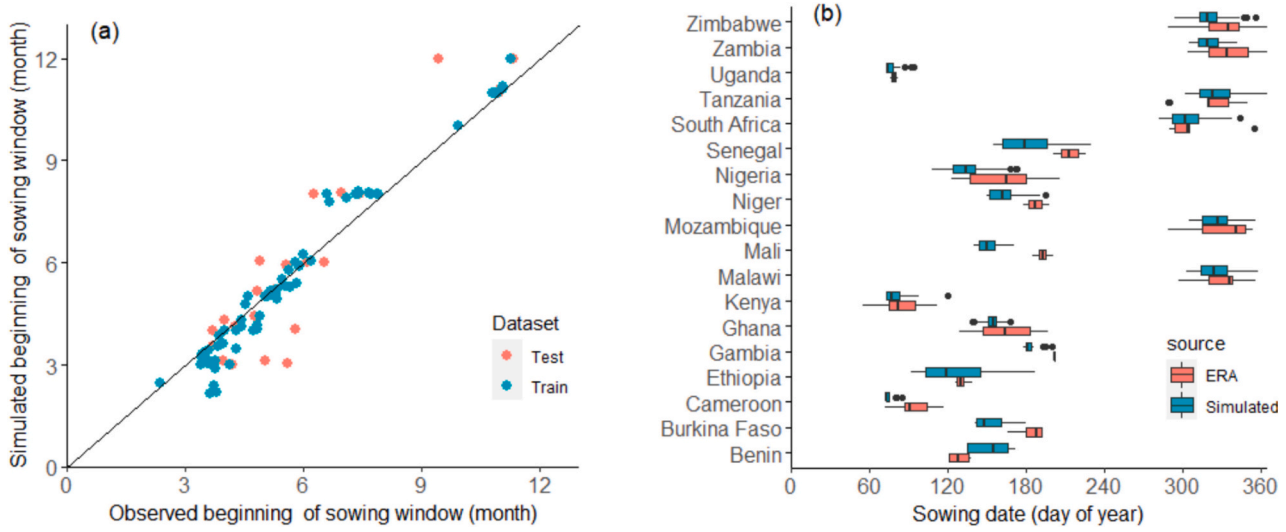

Fig. 2. (a) The simulated beginning of the sowing window using the RF1 model for each representative weather station (blue training dataset, red testing dataset), compared to the observed time for the RWSs. The black line is the 1:1 line; (b) A comparison between the simulated sowing date across different locations using the RF1 model for virtual weather stations within each country and the measured data extracted from the ERA dataset (422 data points) for the relevant virtual weather stations. The simulated results include the historical annual results (1995-2014) at each virtual weather station. (For interpretation of the references to colour in this figure legend, the reader is referred to the web version of this article.)

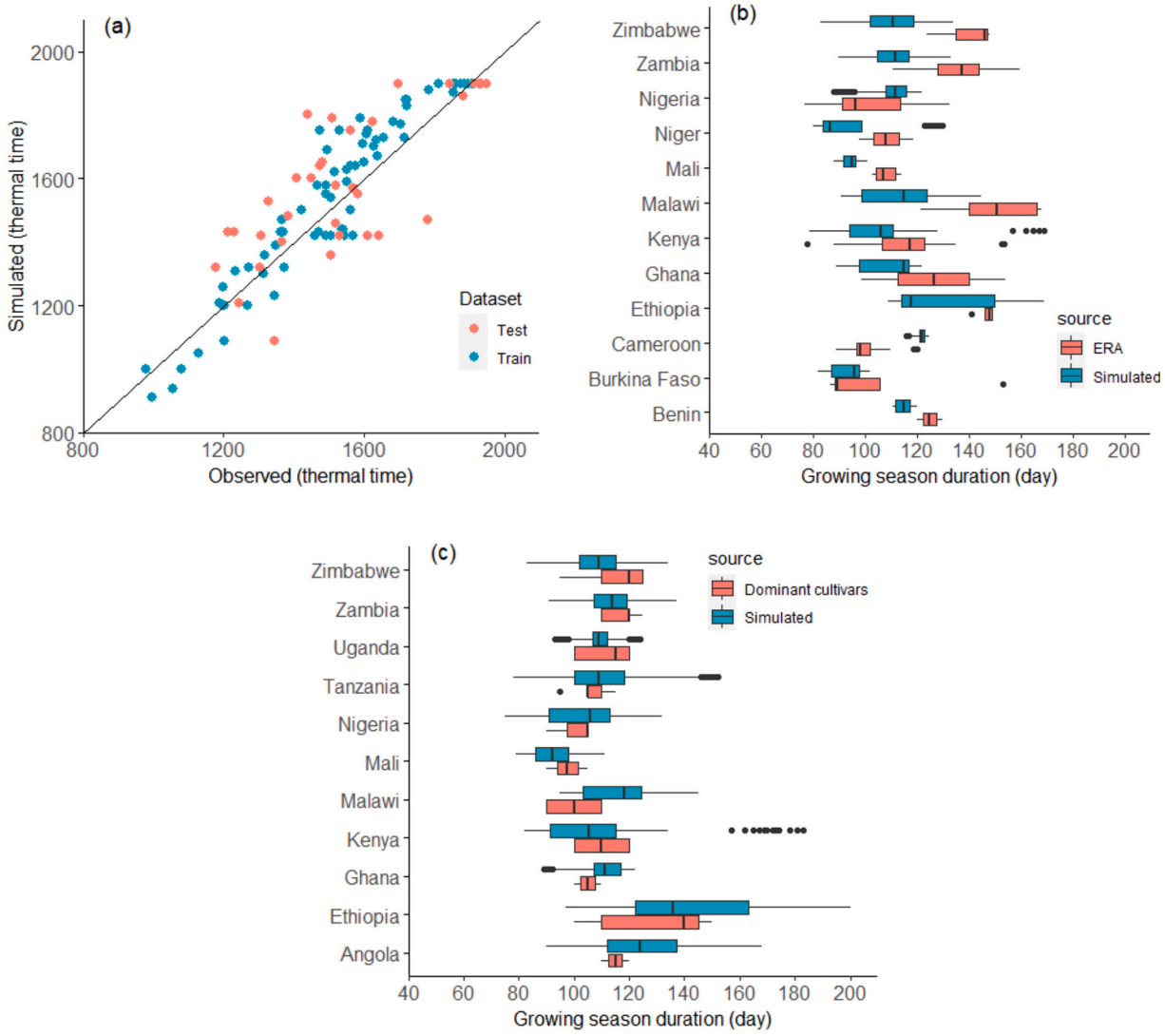

Fig. 3. (a) Simulated output of the required thermal time from sowing to maturity for maize cultivars using the RF2 model versus the GYGA data ('observed') in each RWS. The black line represents the 1:1 line; (b) A comparison of the simulated growing season duration of maize in different VWSs with the observed data extracted from the ERA dataset; (c) Comparison of the simulated growing season from sowing to maturity of maize in dominant regions (in terms of area) with reported durations by seed companies for dominant cultivars in each country (Table S2). Note that, due to differences in the sources of observed data for panels b and c, the lists of countries are not identical.

plus the algorithm to determine the sowing date, RF2 plus the algorithm to derive the phenology and RF3, the yield model; Fig. 1), the simulated rainfed potential yields of the designed system were compared to the experimental yields from the ERA dataset across SSA (Fig. 4). The comparison of the two datasets across different VWSs in different countries highlighted some level of agreement, taking into account that yields from the ERA dataset will be lower than water-limited potential yields (Fig. 4).

The statistical indices (Table 4) and dispersion of points around the one-to-one line in Fig. 5 (and also for SSP3–7.0 in Fig. S4) suggest that the RF3 model can accurately replicate the yields simulated by the WOFOST model, as extracted from Alimagham et al. (2024b). The RF3 model shows a small tendency to overestimate yields, occurring in about 5 % of all simulated yields in SSA. This occurs mostly, for all three time horizons, when yields are below 4 ton/ha. Approximately 12 % of all estimated yields were below 4 ton/ha for all RWSs, and of which 45 % of the cases was overestimated. This indicates the RF3 model's capacity to effectively replicate yields simulated with WOFOST, in at least 95 % of the cases both under SSP5–8.5 and SSP3–7.0 climate change scenarios in all RWSs. These cases differ less than 20 % of those simulated with WOFOST model with high-quality inputs.

3.2. Sensitivity analysis

The rainfed potential yields simulated with the WOFOST model do not show significant differences between the GCMs, and the RF3 outputs produce similar results under both climate change scenarios (Fig. S5). However, the impact of soil depth on yields is substantial. The WOFOST model shows lower yields for shallow soils, and the RF3 model also captures this in all RWSs under historical and both SSP5–8.5 and SSP3–7.0 climate change scenarios (Fig. S6).

The RF3 model is also capable of effectively mimicking the WOFOST model's yields for climate change of different time horizons (Fig. 5 and S4). Thus, the difference in performance between the two methods under low yields is not likely to be attributable to the impact of temperature and/or CO_2 concentration. Nonetheless, a divergence in cumulative distributions is illustrated for yields below 4 ton/ha, particularly for shallow soils (Fig. S6). It appears the main contributing factor to the disparity in low yields between the two methods is associated with the water balance, given the significant impact of maximum

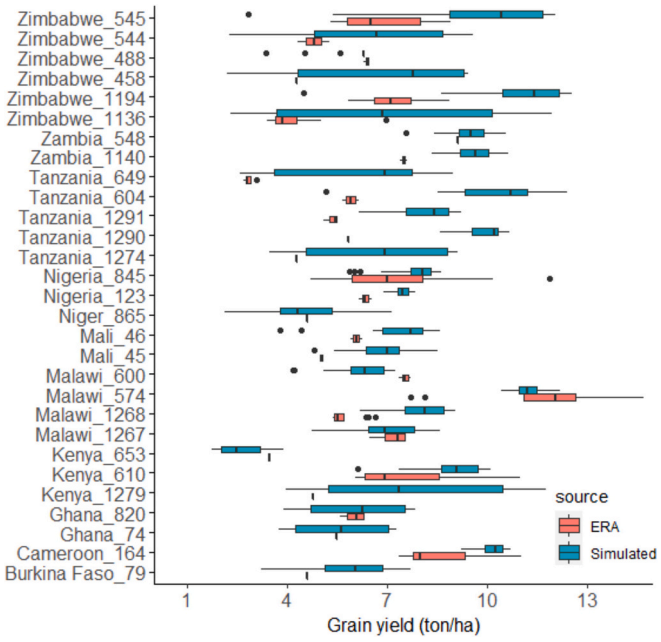

Fig. 4. Comparison between the simulated rainfed potential maize yield across different locations using the system presented in Fig. 1 and the measured data extracted from the ERA dataset. The simulated results include the historical annual results (1995-2014) from five GCMs at each site. The numerical values on the y-axis represent the code of virtual weather stations in each country; Fig. S7 presents the same results but at the country level.

rootable soil depth on water storage capacity. We further examined this assumption (Fig. 6 and 7). The largest discrepancy between the RF3 and WOFOST yields clearly occurs with low rainfall during the various growth stages. Thus, this suggests that the disparity between the two methods at low yields can be attributed to factors related to drought during the growing season (Fig. 6). Warmer conditions also lead to a slight increase in the disparity (Fig. 7). Despite its restriction to a limited section within Fig. 7 (specifically, the area denoted in purple), Fig. 6 exhibits this divergence across a more extensive range of percentages. Thus, the role of temperature is less significant compared to drought stress at indicating these variations (Fig. 6 and 7). Furthermore, regions with high temperature typically experience less rainfall in SSA, so the disparity seen in Fig. 7 can also be a result of drought stress.

3.3. *Coverage of different climate zones and maize area in entire SSA*

The coverage of climate zones with maize land in the training dataset is important, as there is a possibility of significant uncertainty when extrapolating outcomes across the entire SSA when not all climate zones are adequately presented. Our results indicate that a climate zone in southern Africa with relatively low temperatures and dry conditions, does not have a RWS in the training dataset (Fig. 8 and 9a). This climate zone includes ca. 3 % of the total maize area in SSA. It is important to mention that South Africa has a large temperature fluctuation throughout the year. The cultivation of maize occurs during summer, when temperatures are highest, so the low temperatures in South Africa are not an issue. Note, that our components are trained with the environmental conditions experienced during the maize growing season, rather than with the annual indices. Thus, the environmental conditions during the maize growing season in South Africa resemble those in other regions such as in East Africa, despite differences in climate zone characteristics based on annual indices. Thus, our dataset includes all

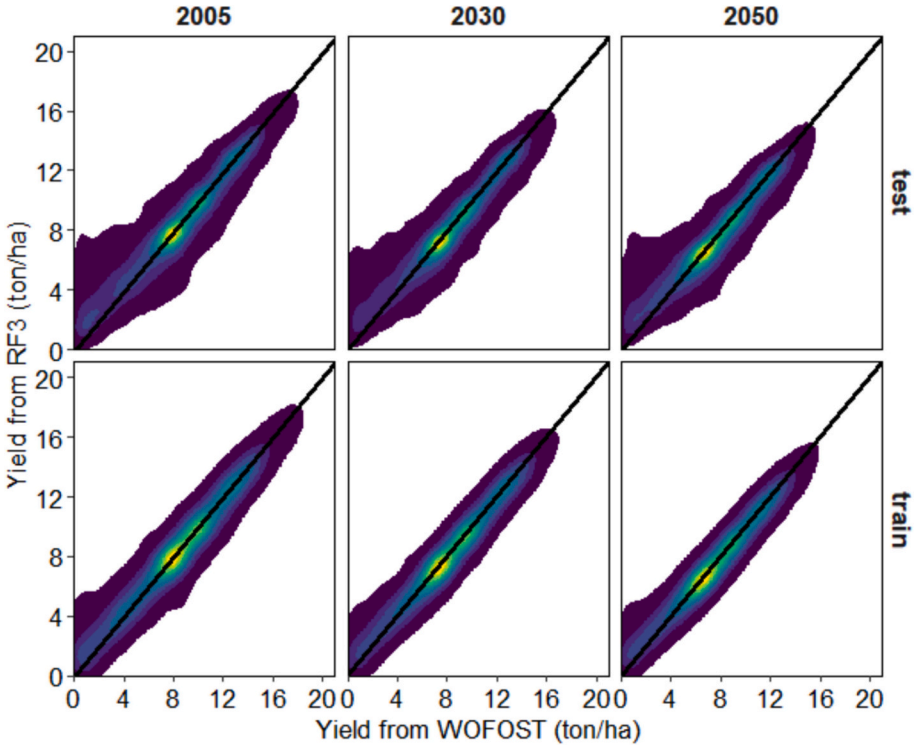

Fig. 5. Comparison of the rainfed potential maize yields simulated with RF3 and with WOFOST for the training (approx. 54,000 points) and test sets (approx. 216,000 points) for different time horizons under the historical conditions (2005) and climate change scenario SSP5–8.5 (2030 and 2050) for the future time horizons. The charts present annual outcomes for a combination of 5 GCMs, 103 weather stations, various soil types within each station's buffer zone and mono or double cropping for maize in the GYGA dataset. The colours represent point density fractions, with each colour representing 10 % of the total points; The same information is presented in Fig. S4, but for the SSP3–7.0 climate change scenario.

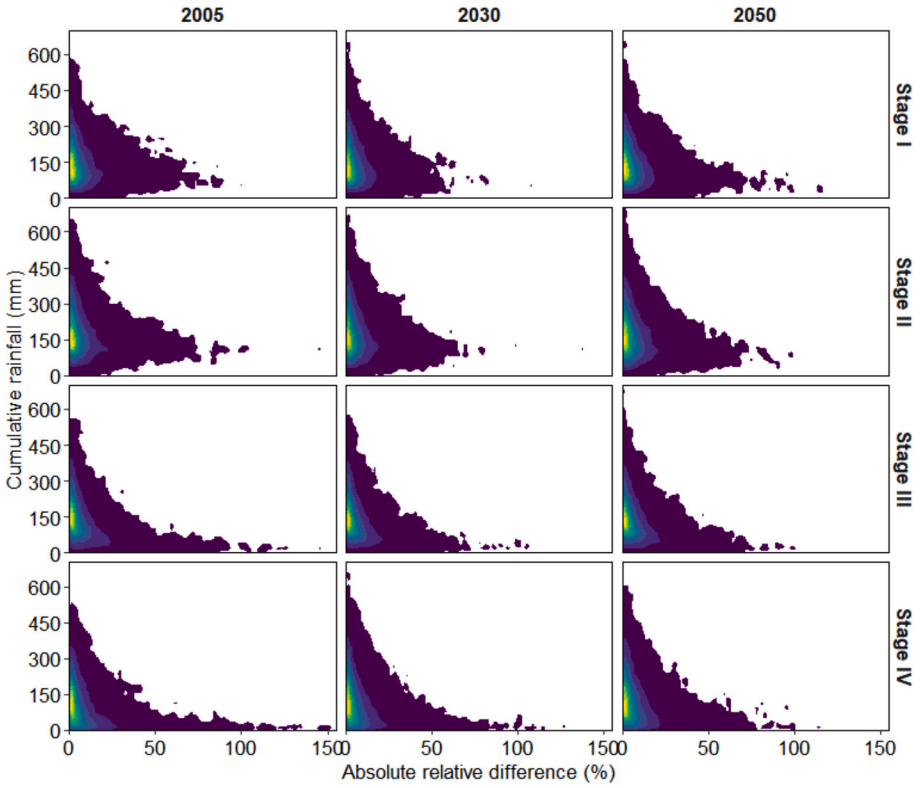

Fig. 6. The relationship between the absolute relative rainfed potential yield differences between RF3 and WOFOST (|(RF3-WOFOST)/WOFOST*100|) and cumulative rainfall during each growth stage of maize under the SSP5–8.5 climate change scenario. The colors indicate point density fractions, with each color representing 10% of the total dataset (approximately 134,000 points per chart).

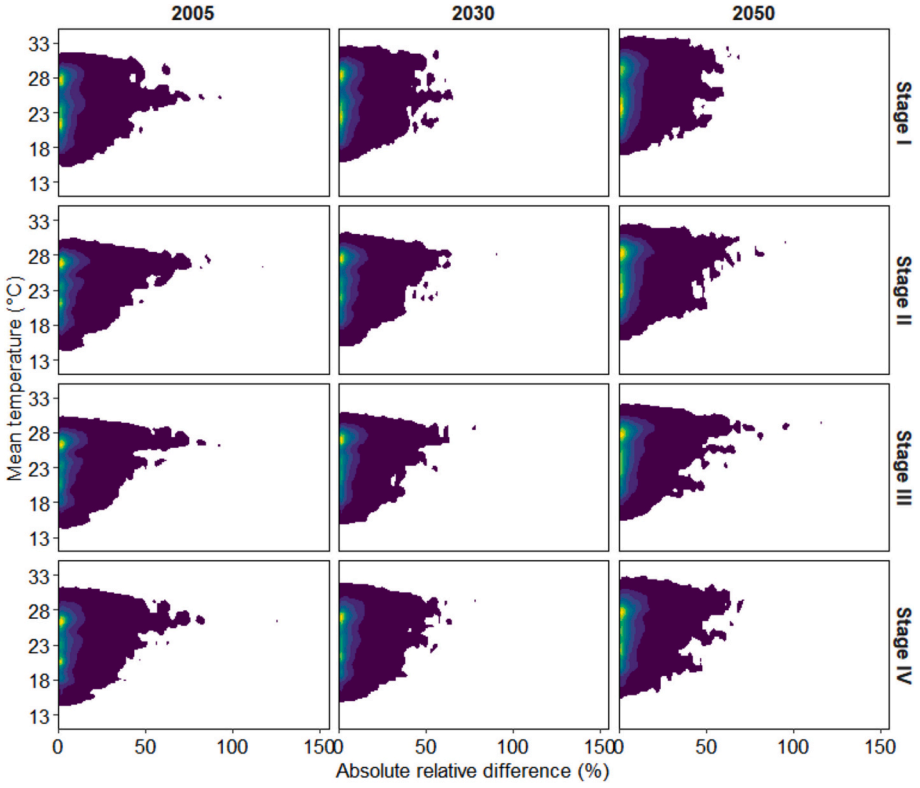

Fig. 7. The relationship between the absolute relative rainfed potential yield differences between RF3 and WOFOST (|(RF3-WOFOST)/WOFOST*100|) and average temperature during each growth stage of maize under the SSP5–8.5 climate change scenario. The colors indicate point density fractions, with each color representing 10% of the total dataset (approximately 134,000 points per chart).

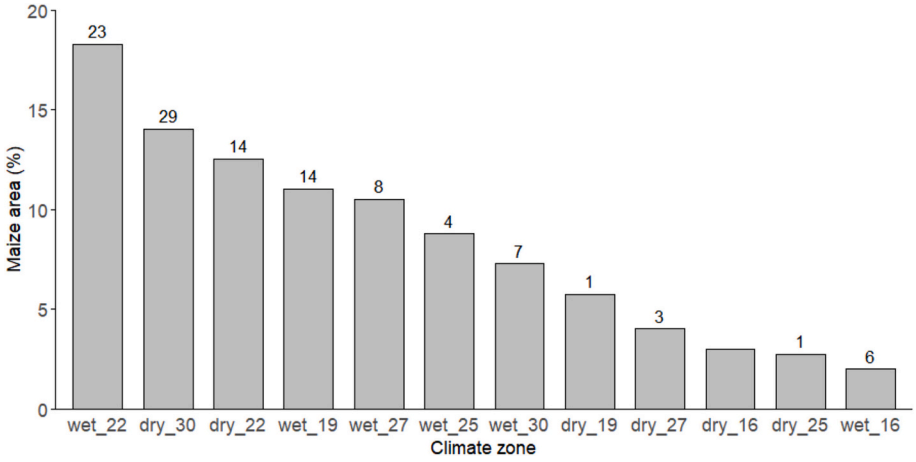

Fig. 8. Percentage of total maize cultivation area in sub-Saharan Africa situated within each climate zone. The numbers on top of the bars show the numbers of RWSs located in each climate zone (Fig. S1 and S9). A dry climate zone was defined as one where annual cumulative potential evapotranspiration fell below 30 % of total annual precipitation. The numerical values in the names of climate zones indicate the annual mean temperature associated with each zone. Fig. S9 presents the spatial distribution of these climate zones across SSA.

historical climate conditions for training the algorithms. However, according to the results, ca. 21 % of climate zones (in terms of maize harvested area) in SSA are exposed to new environmental conditions in future climates (Fig. 9b). These regions are all located in the northern part of SSA. Annual temperatures in these climate zones surpass historical maximum ranges due to the impacts of climate change. It is worth noting that the degree of uncertainty in the results within these specific regions may be greater compared to other regions.

3.4. Examples of the framework's modeling outputs

The geographically continuous gridded projections by the framework of the growing season duration and the rainfed potential yields of common maize cultivars are illustrated by Fig. 10. Furthermore, it presents the impact of climate change on the duration of the growing season and rainfed potential yields in 2050 compared to historical conditions. The results indicate that the sites with dry climates have the shortest growing season durations (Fig. 10a and S9). It is projected that the growing season of maize will be reduced by 0 to 35 days due to climate change across SSA in 2050 (Fig. 10b). The regions with lower mean temperatures, such as the western part of Ethiopia, certain regions in South Africa, and the north of Angola, are projected to experience the most significant decrease in the duration of the maize growing season in 2050 compared to the historical conditions (Fig. 10b).

The spatial distribution of simulated rainfed potential yields align with the climate conditions in SSA. The areas mentioned in the previous paragraph that have a dry climate has the lowest yields. Conversely, regions such as the western part of Ethiopia, which have mild temperatures and wet climate conditions, have the highest yields (Fig. 10c; Fig. S9). In comparison to historical conditions, the rainfed potential yields in 2050 are up to 44 % lower or up to 116 % higher due to the effects of climate change. The regions with the greatest positive relative

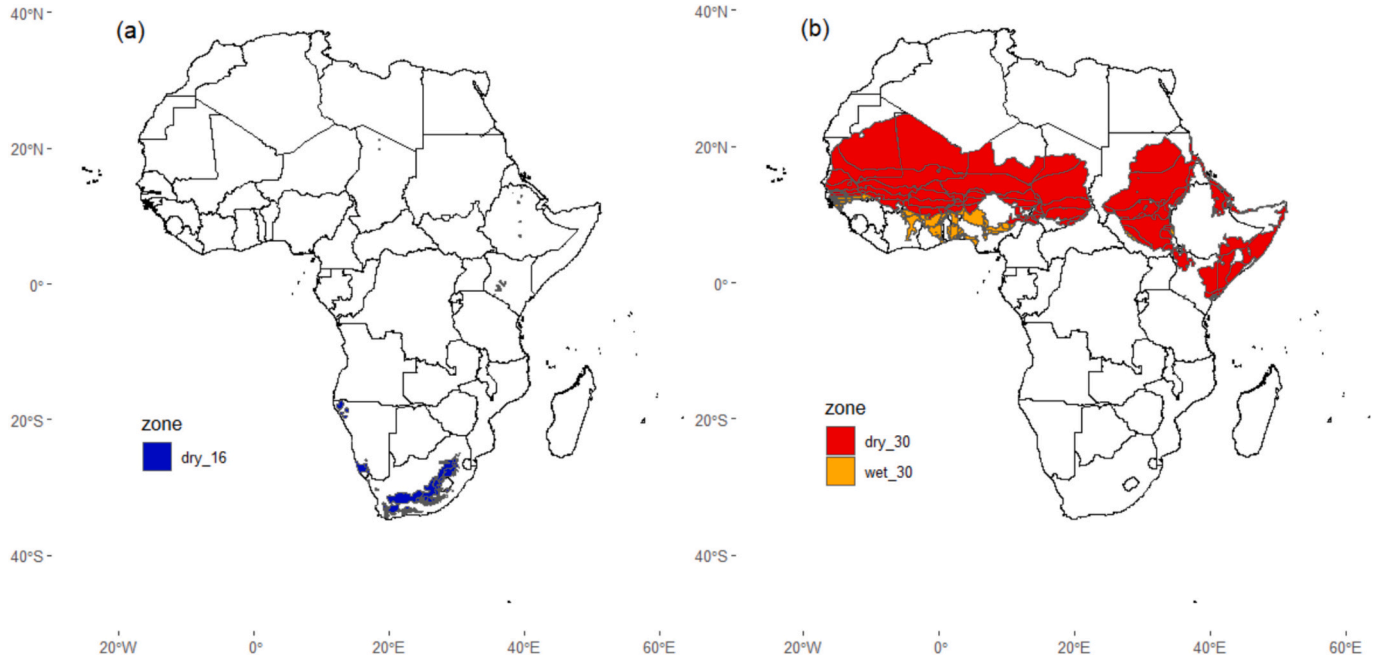

Fig. 9. (a) the climate zone which is not represented by the GYGA reference weather stations under historical conditions; (b) the zones in SSA that exhibit warmer climates in the future and those warmer climates are not adequately represented by the current GYGA's reference weather stations.

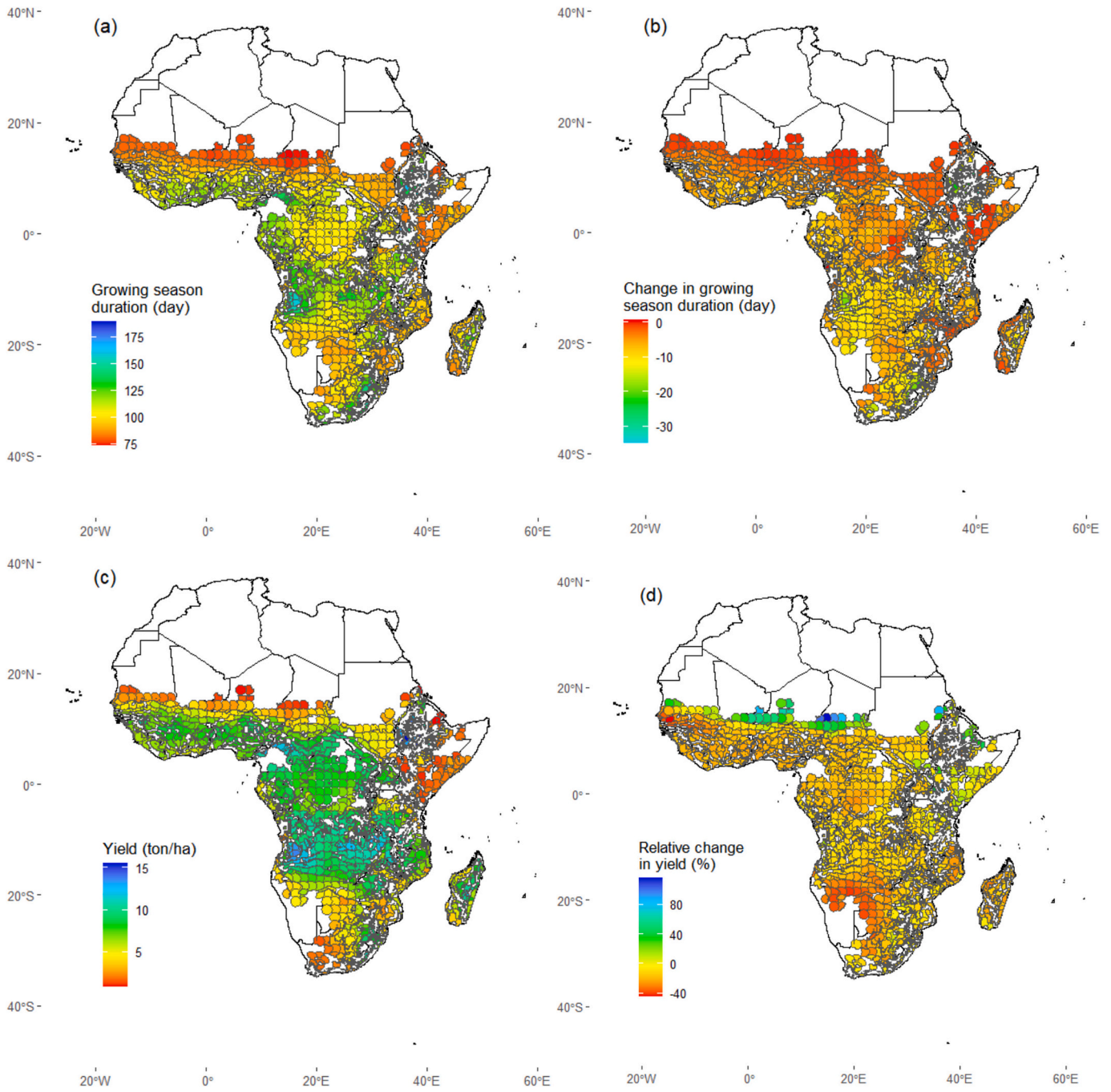

Fig. 10. (a) Simulated growing season duration of maize across SSA under historical conditions in the main season; (b) the projected change in the maize growing season duration in 2050, when compared to historical conditions; (c) simulated rainfed potential yield of maize across SSA under historical conditions; (d) the projected relative change in the rainfed potential yield in 2050, when compared to historical conditions. The results shown in these panels are based on MPI weather data and the SSP5–8.5 climate change scenario. Yield is expressed in dry weight.

impacts are observed in areas with extremely low rainfed potential yields (less than 1.5 ton/ha) under historical conditions, specifically in the northern part of SSA (Fig. 10c and d). Therefore, absolute yield changes of 1 to 2 tons/ha due to climate change impacts are equivalent to substantial changes in relative yield in these areas. It is projected that a significant number of sites in SSA will face a decline in rainfed potential yield of maize, ranging from 10 % to 20 % (Fig. 10d).

4. Discussion

4.1. Combining the strengths of process-based crop models and machine learning

In this study we presented an approach that capitalises on the strengths of a mechanistic crop growth model, relatively high-quality input data from key production areas in a subset of countries in SSA, and machine learning to allow for extrapolation of yields to the entire sub-continent. Substantial effort was put into key eco-physiological parameters and processes, including sowing date window, sowing

date, crop phenology and four different growth stages of the crop during which temperature and water stress may have distinct effects. The proposed approach relies on high quality input data for a limited number of locations, but it does not need such high-quality data for extrapolation to other locations. This is particularly appealing to data-scarce regions such as SSA. While we used the crop growth model WOFOST for generating input data, this approach can use inputs from results of any well-tested crop growth model. The same holds for the choice of a machine learning method. Based on previous studies indicating that Random Forest can successfully simulate crop yields, we opted for this method for our study (Aramburu-Merlos et al., 2024; Lischeid et al., 2022; Van Klompenburg et al., 2020; Jeong et al., 2016). Comparison of the results of our framework using the crop model and Random Forest with simulation results derived from the crop model employing robust input data demonstrated that our approach can be used with high accuracy. Yet, the approach presented in the current study is flexible, allowing for different combinations of machine learning techniques and crop simulation models based on the user's expertise, familiarity with various methods, and the performance of these tools in the target regions.

4.2. The advantages of the approach

Despite the fact that the greatest differences between the rainfed potential yields estimated by RF3 and WOFOST occurred under conditions of low rainfall, there are still many points with minimal differences between the two models for these specific conditions (Fig. 5). In some cases the RF3 model produced better yield simulations as compared to WOFOST. For example, at Wolkite in Ethiopia in 2005, the maize yield simulated by WOFOST was 0.08 ton/ha, while for the RF3 it was 6.3 ton/ha. Here, WOFOST failed to accurately simulate potential rainfed conditions, as simulated yields were much lower than actual farmers' yields observed at that location (around 2.8 ton ha^{-1}), let alone the rainfed potential yield of the region. In this particular case, the crop simulated with WOFOST did not produce any leaf area throughout the entire growing season, resulting in a lack of simulated transpiration (Fig. S8). However, the evaporation rate from the soil surface during the entire season was within the usual range (Fig. S8). In this case, the failure of WOFOST to produce sufficient leaf area and grain can be attributed to the drizzling bias effect during the early growing season. Climate models often overestimate precipitation frequency and duration, but underestimate its intensity, resulting in a drizzling bias (Chen et al., 2021). The issue of accurately representing drizzling bias has been a longstanding challenge for global climate models (Chen et al., 2021). Using cumulative rainfall data in four distinct crop growth phases and ML, as done in our proposed methodology, can be considered a promising approach to tackle this issue.

Two sets of data were used in this study to evaluate the algorithms of our approach: the GYGA data for RWSs and the ERA field experimental data. The simulated results from the new approach are consistent with all data from the GYGA dataset and the sowing dates provided by the ERA dataset. However, in some VWSs (that is for regions in SSA for which no RWSs were applicable), we found significant differences between the simulated data and the extracted data from the ERA dataset (Fig. 3b). Generally, measured durations of the growing season in the ERA dataset are longer than the simulated values. In our approach, we define the growing season as the period from sowing to maturity. However, the ERA data experiments, which encompassed both on-farm and on-station experiments, defines the growing season as the period from sowing to harvesting time. The time of harvesting does not necessarily correspond to the time of the maturity, especially in on-farm experiments in SSA where harvesting typically takes place a considerable time after maturity has been reached (Asare et al., 2023; Kaaya et al., 2005; Alakonya et al., 2008).

In previous large-scale studies in SSA, the time from sowing to harvesting obtained from different sources has been used as the growing season duration in simulations using crop models (Jägermeyr et al., 2021; Zabel et al., 2021) or ML techniques (Aramburu-Merlos et al., 2024) to simulate potential yields. When the growing season is prolonged due to delayed (relative to maturity) harvesting, as suggested in Fig. 3b and c, the simulations are using too long a growing season for training the simulations. This could be considered a potential source of error in simulations in large-scale studies. Additionally, considering the impact of climate change on growing season duration (Fig. 10b; Cleland et al., 2007), using an incorrect growing season duration and timing in yield simulations could lead to significant uncertainties under future climate conditions. We demonstrated that our approach is capable of accurately estimating the duration from sowing to maturity across SSA (Fig. 3a,c). Thus, the outputs from the two crop model algorithms (A1 and A2) can be reliably used for future crop modeling- or ML-based studies in SSA under current and future climate conditions. Furthermore, dividing the growing season into four periods allows for capturing various stress patterns during the growing season, including early-season, mid-season, and late-season stress (Table 2).

4.3. Limitations

Crop model outputs were evaluated at the local level in the GYGA project under historical climate conditions (Rattalino Edreira et al., 2021; Alimagham et al., 2024a and b). The algorithms presented in this paper are trained using data from the GYGA dataset, encompassing all significant (in terms of area) climate zones relevant to maize cultivation in SSA under historical conditions. Also, these climate zones represent 79 % of the climate zones (in terms of area for maize) under future climate conditions according to the CMIP6 weather data. Thus, the GYGA dataset serves as a valuable resource used in our study to train algorithms for SSA under both historical and future climate conditions. Yet, we caution to use our approach for future climates that do not currently exist and hence for which the approach has not been trained (Meyer and Pebesma, 2022). To improve this, we aim to enrich the GYGA data with data from hot regions in northern parts of SSA during extreme warm years and to use these for training our framework in future efforts.

In West Africa, farmers generally tend to sow maize after the first main rainfall (greater than 20 mm) at the onset of the rainy season (Agbossou et al., 2012; Akponikpè et al., 2010). The algorithm used to estimate sowing date in this study calculates the cumulative rainfall over seven consecutive days within the sowing window. The last day of this period, resulting in more than 20 mm cumulative rainfall, is considered the sowing date. Therefore, the algorithm we used in this study is less conservative compared to the farmers' approach of sowing when rainfall exceeds 20 mm in a day, which can lead to a later sowing date. The more conservative algorithm for maize sowing used by farmers in West Africa may be due to the high cost of maize seeds (Adigoun et al., 2022), with farmers attempting to mitigate the potential risks of early-season drought stress by sowing slightly later. Thus, identifying country-specific sowing date algorithms that incorporate local management factors in addition to environmental factors could enhance the accuracy of sowing date determination in future studies, particularly in West Africa.

Although we filtered the ERA dataset for experiments with the highest yields (Table 3), the majority of them fell short to apply enough nitrogen fertilizer to reach potential rainfed yields (Fig. S10). As a result, it is most likely that the filtered ERA yields are below their potential rainfed yields, which is also shown by our approach as our simulated yields are usually higher than those from the ERA dataset (Fig. 4). Nevertheless, we employed the ERA dataset to evaluate our framework in terms of spatial distribution of yields. Evidently, any future modeling efforts for SSA will benefit from well-managed experiments targeting (water-limited) potential yields.

4.4. Further applications of the approach

It has been reported that statistical models and ML-based models possess the capacity to capture extreme impacts, without requiring a complex parameter set or an extensive understanding of eco-physiological processes (Feng et al., 2019). However, mechanistic crop models can account for eco-physiological processes better than statistical and ML-based models (Roberts et al., 2017). Thus, the combination of mechanistic crop models and ML algorithms guided by eco-physiological principles holds the potential for improving simulation accuracy under climate change conditions, particularly when addressing the impacts of extreme conditions (Bai et al., 2024; Kumari et al., 2024; Zhu et al., 2021). However, to fully exploit this potential, it is necessary to have high-quality experimental yield data obtained under extreme conditions (Kim et al., 2024; Rötter et al., 2018), which is currently a severe limitation in SSA and for other regions.

Our proposed and tested framework is able to simulate both potential yields (irrigated conditions; results were not shown) and rainfed potential yields (rainfed conditions). The ratio of the rainfed potential yield to the potential yield can serve as a drought stress index (Van Oort, 2018), allowing our approach to identify a crop- and site-specific water stress severity map across SSA under current and future climate conditions. This map holds significant importance in the field of breeding and crop management practices (Jha et al., 2023; Rizza et al., 2004; Debaeke and Aboudrare, 2004). In addition, by using data from different GCMs or climate change scenarios, our approach enables the analysis of uncertainty in the results under climate change conditions (Tao et al., 2018).

Altering the sowing dates and incorporating new cultivars in terms of maturity group are acknowledged as promising approaches to adapt to climate change conditions in SSA (Alimagham et al., 2024a; Carr et al., 2022; Zabel et al., 2021). Our method can be used to assess the influence of these factors across SSA under climate change conditions. Due to its ability to capture the timing and duration of phenological stages, the approach can be employed to assess different cultivars with varying growing season durations across SSA under current and future climate conditions. By modifying the outputs obtained from the RF2 model, which simulates the thermal time requirement of the current cultivars, it is possible to adjust the thermal time required from the sowing until the flowering, and from the flowering to the maturity, either separately or jointly under current and future climate conditions. After adjusting thermal time requirements provided by the RF2 model, the rainfed potential yield can be simulated using the new phenological data.

Evaluating potential impacts of climate change on agricultural commodities plays a key role in informing policy decisions globally (IPCC, 2023). When combined with other factors, such as rising sea levels, heat-humidity risks to human health, and more, this information provides valuable insights. Such insights are crucial for addressing challenges such as land competition between urban expansion and food production, conflicts between nations over food resources and population migration patterns in the context of climate change (IPCC, 2023). This requires detailed information on the potential impacts of climate change for all key crops, rather than focusing on just a few crops. By strategically narrowing the focus of data collection and crop model evaluation to specific regions in SSA, such as done with the GYGA protocol (Grassini et al., 2015; van Bussel et al., 2015) the presented approach allows to generate accurate and reliable output (phenology and crop yields) for different crops for the entire SSA. Our approach is not only valid for maize, but could also serve as a basis for exploring potential food production of all major food crops in SSA now and under climate change conditions. In addition, the presented approach allows to test the effect of adaptation of crop cultivars in terms of maturity group. Applications of our approach to the purpose of climate change adaptation are visualized in the Africa Agriculture Adaptation Atlas for multiple crops, i.e. maize, millet, sorghum, wheat, soybean, groundnut, common bean and cowpea (https://observablehq.com/d/4c65e6dd0bfc32a5). The Africa Agriculture Adaptation Atlas seeks to curate and enhance scientific knowledge on climate adaptation in Africa, aiming to create a comprehensive resource for investors, policymakers, and researchers (https://adaptationatlas.cgiar.org/).

Potential impacts of climate change on rainfed yield potentials represent a key strategic indicator for research and development in SSA. It provides an upper benchmark to, for example, nutrient-limited yields (Falconnier et al., 2020). Such data are essential for policymakers in crafting scenarios that address food security in the context of future climate conditions. With projections suggesting that food demand will increase two- to threefold over the next three decades, achieving the needed yield growth in SSA is critical (Van Ittersum et al., 2016). Consequently, the benchmark of rainfed yield potential becomes increasingly significant: a decline in this benchmark signals a potential future threat to regional food security. By projecting this challenge, policymakers can be better equipped to respond proactively and strategically.

5. Conclusion

While accounting for eco-physiological principles, we integrated machine learning techniques with two crop model algorithms to simulate the rainfed potential yield across SSA. For locations where we could rely on detailed crop growth simulations using local data and the WOFOST crop model, our approach was robust in 95 % of the cases. The approach can also improve crop growth simulations, particularly in addressing biases in rainfall data associated with the so-called "drizzling effect." The algorithms are trained using observed data from a limited number of carefully chosen locations in SSA. Based on our analysis, we conclude that the approach can be used for yield estimation under both current and future climate conditions, using data from various GCMs or different soil types. Furthermore, the approach can be applied to a variety of crops for which detailed, tested, simulations are available at a range (yet limited number) of locations. Thus, the technique outlined in this study can extrapolate crop growth simulations to virtually all conditions occurring in SSA's maize lands with high accuracy for different crops, and with far fewer data requirements compared to process-based crop models.

CRediT authorship contribution statement

Seyyedmajid Alimagham: Writing – original draft, Software, Methodology, Data curation, Conceptualization. **Marloes P. van Loon:** Writing – original draft, Data curation. **Julian Ramirez-Villegas:** Writing – original draft, Conceptualization. **Herman N.C. Berghuijs:** Writing – review & editing, Methodology. **Todd S. Rosenstock:** Writing – review & editing. **Martin K. van Ittersum:** Writing – original draft, Supervision, Conceptualization.

Declaration of competing interest

The authors declare that they have no known competing financial interests or personal relationships that could have appeared to influence the work reported in this paper.

Acknowledgement

This work was supported, in whole or in part, by the Bill & Melinda Gates Foundation [Grant Number INV-029211]. Under the grant conditions of the Foundation, a Creative Commons Attribution 4.0 Generic License has already been assigned to the Author Accepted Manuscript version that might arise from this submission.

Appendix A. Supplementary data

Supplementary data to this article can be found online at https://doi.org/10.1016/j.agsy.2025.104367.

Data availability

Data will be made available on request.

References

Abate, T., Fisher, M., Abdoulaye, T., Kassie, G.T., Lunduka, R., Marenya, P., Asnake, W., 2017. Characteristics of maize cultivars in Africa: how modern are they and how many do smallholder farmers grow? Agric. Food Secur. 6, 1–17.

Abrams, L., 2018. Unlocking the Potential of Enhanced Rainfed Agriculture. Stockholm International Water Institute, Stockholm.

Adigoun, R.F., Houdegbe, A.C., Fassinou Hotegni, N.V., Segnon, A.C., N'Danikou, S., Adjé, C.A., Adadja, R.P., Achigan-Dako, E.G., 2022. Enabling effective maize seed system in low-income countries of West Africa: insights from Benin. Front. Sustain. Food Syst. 6, 1045629.

Agbossou, E.K., Toukon, C., Akponikpè, P.B.I., Afouda, A., 2012. Climate variability and implications for maize production in Benin: A stochastic rainfall analysis. Afr. Crop. Sci. J. 20, 493–503.

Agossou, C., Kang, S., 2020. Climatic factors controlling interannual variability of the onset of vegetation phenology in the northern sub-Saharan Africa from 1988 to 2013. Afr. J. Ecol. 58 (2), 299–308.

Akponikpè, P.I., Gérard, B., Michels, K., Bielders, C., 2010. Use of the APSIM model in long term simulation to support decision making regarding nitrogen management for pearl millet in the Sahel. Eur. J. Agron. 32 (2), 144–154.

Alakonya, A.E., Monda, E.O., Ajanga, S., 2008. Effect of delayed harvesting on maize ear rot in Western Kenya. Am. Eurasian J. Agric. Environ. Sci. 4, 372–380.

Alimagham, S., van Loon, M.P., Ramirez-Villegas, J., Adjei-Nsiah, S., Baijukya, F., Bala, A., Chikowo, R., Silva, J.V., Soulé, A.M., Taulya, G., Tenorio, F.A., Tesfaye, K. and van Ittersum, M.K. 2024a a. Climate change impact and adaptation of rainfed cereal crops in sub-Saharan Africa. Eur. J. Agron., 155, p.127137.

Alimagham, S., van Loon, M.P., Ramirez-Villegas, J., Berghuijs, H.N. and van Ittersum, M.K., 2024b b. Daily bias-corrected weather data and daily simulated growth data of maize, millet, sorghum, and wheat in the changing climate of sub-Saharan Africa. Data Brief, 54, p.110455.

Aramburu-Merlos, F., van Loon, M.P., van Ittersum, M.K., Grassini, P., 2024. High-resolution global maps of yield potential with local relevance for targeted crop production improvement. Nat. Food 1–6.

Asare, S.G., Abankwa-Kwarteng, S., Owusu, B.S., Baidoo, P.K., 2023. Effects of harvest time on quality of stored maize (Zea mays L.) in the southern part of Ghana. *Peruvian*. J. Agron. 7 (2), 144–155.

Asseng, S., Ewert, F., Martre, P., Rötter, R.P., Lobell, D.B., Cammarano, D., Kimball, B.A., Ottman, M.J., Wall, G.W., White, J.W., Reynolds, M.P., 2015. Rising temperatures reduce global wheat production. Nat. Clim. Chang. 5 (2), 143–147.

Bai, H., Xiao, D., Tang, J., Li Liu, D., 2024. Evaluation of wheat yield in North China plain under extreme climate by coupling crop model with machine learning. Comput. Electron. Agric. 217, 108651.

Boogaard, H. and van der Grijn, G., 2020. Product user guide and specification. Data stream 2: AgERA5 historic and near real time forcing data, global agriculture.

Breiman, L., 1996. Bagging predictors. Mach. Learn. 24, 123–140.

Breiman, L., 2001. Random forests. Mach. Learn. 45, 5–32.

Büchner, M., Reyer, C., 2022. ISIMIP3b Atmospheric Composition Input Data (v1. 1). ISIMIP Repository.

Cakir, R., 2004. Effect of water stress at different development stages on vegetative and reproductive growth of corn. Field Crop Res. 89 (1), 1–16.

Calviño, P.A., Andrade, F.H., Sadras, V.O., 2003. Maize yield as affected by water availability, soil depth, and crop management. Agron. J. 95 (2), 275–281.

Carr, T.W., Mkuhlani, S., Segnon, A.C., Ali, Z., Zougmoré, R., Dangour, A.D., Green, R., Scheelbeek, P., 2022. Climate change impacts and adaptation strategies for crops in West Africa: a systematic review. Environ. Res. Lett. 17 (5), 053001.

Cavus, Y., Stahl, K., Aksoy, H., 2023. Drought intensity–duration–frequency curves based on deficit in precipitation and streamflow for water resources management. Hydrol. Earth Syst. Sci. 27 (18), 3427–3445.

Chen, Y.C., Wang, S.H., Min, Q., Lu, S., Lin, P.L., Lin, N.H., Chung, K.S., Joseph, E., 2021. Aerosol impacts on warm-cloud microphysics and drizzle in a moderately polluted environment. Atmos. Chem. Phys. 21 (6), 4487–4502.

Cleland, E.E., Chuine, I., Menzel, A., Mooney, H.A., Schwartz, M.D., 2007. Shifting plant phenology in response to global change. Trends Ecol. Evol. 22 (7), 357–365.

De Wit, A., Boogaard, H., Fumagalli, D., Janssen, S., Knapen, R., van Kraalingen, D., Supit, I., van der Wijngaart, R., van Diepen, K., 2019. 25 years of the WOFOST cropping systems model. Agric. Syst. 168, 154–167.

Debaeke, P., Aboudrare, A., 2004. Adaptation of crop management to water-limited environments. Eur. J. Agron. 21 (4), 433–446.

Falconnier, G.N., Corbeels, M., Boote, K.J., Affholder, F., Adam, M., MacCarthy, D.S., Ruane, A.C., Nendel, C., Whitbread, A.M., Justes, É., Ahuja, L.R., et al., 2020. Modelling climate change impacts on maize yields under low nitrogen input conditions in sub-Saharan Africa. Glob. Chang. Biol. 26 (10), 5942–5964.

Fatima, Z., Ahmed, M., Hussain, M., Abbas, G., Ul-Allah, S., Ahmad, S., Ahmed, N., Ali, M.A., Sarwar, G., Haque, E.U., Iqbal, P., 2020. The fingerprints of climate warming on cereal crops phenology and adaptation options. Sci. Rep. 10, 18013.

Feng, P., Wang, B., Li Liu, D., Waters, C., Yu, Q., 2019. Incorporating machine learning with biophysical model can improve the evaluation of climate extremes impacts on wheat yield in South-Eastern Australia. Agric. For. Meteorol. 275, 100–113.

Funk, C., Peterson, P., Landsfeld, M., Pedreros, D., Verdin, J., Shukla, S., Husak, G., Rowland, J., Harrison, L., Hoell, A., Michaelsen, J., 2015. The climate hazards infrared precipitation with stations—a new environmental record for monitoring extremes. Sci. Data 2 (1), 1–21.

Funk, C., Peterson, P., Peterson, S., Shukla, S., Davenport, F., Michaelsen, J., Knapp, K.R., Landsfeld, M., Husak, G., Harrison, L., Rowland, J., 2019. A high-resolution 1983–2016 T max climate data record based on infrared temperatures and stations by the climate Hazard center. J. Clim. 32 (17), 5639–5658.

Ge, T., Sui, F., Bai, L., Tong, C., Sun, N., 2012. Effects of water stress on growth, biomass partitioning, and water-use efficiency in summer maize (Zea mays L.) throughout the growth cycle. Acta Physiol. Plant. 34, 1043–1053.

Grassini, P., van Bussel, L.G., Van Wart, J., Wolf, J., Claessens, L., Yang, H., Boogaard, H., de Groot, H., van Ittersum, M.K., Cassman, K.G., 2015. How good is good enough? Data requirements for reliable crop yield simulations and yield-gap analysis. Field Crop Res. 177, 49–63.

Guo, Y., Fu, Y., Hao, F., Zhang, X., Wu, W., Jin, X., Bryant, C.R., Senthilnath, J., 2021. Integrated phenology and climate in rice yields prediction using machine learning methods. Ecol. Indic. 120, 106935.

Hasegawa, T., Wakatsuki, H., Ju, H., Vyas, S., Nelson, G.C., Farrell, A., Deryng, D., Meza, F., Makowski, D., 2022. A global dataset for the projected impacts of climate change on four major crops. Sci. Data 9 (1), 58. https://adaptationatlas.cgiar.org/ (available on 22-10-2024), https://cran.r-project.o rg/web/packages/tidyverse/index.html, https://cran.r-project.org/web/packages/caTools/index.html, https://github.com/ajwdewit/WOFOST_crop_parameters (available on 22-10-2024), https://observablehq.com/d/4c65e6dd0bfc32a5 (available on 22-10-2024), https://www.freemaptools.com/elevation-finder.htm (available on 22-10-2024), https://www.yieldgap.org/ (available on 22-10-2024), https://www.yieldgap.org/web/guest/climate-zones (available on 22-10-2024).

Hu, J., Zhao, X., Gu, L., Liu, P., Zhao, B., Zhang, J., Ren, B., 2023. The effects of high temperature, drought, and their combined stresses on the photosynthesis and senescence of summer maize. Agric. Water Manag. 289, 108525.

International Food Policy Research Institute (IFPRI), 2024. Global spatially-disaggregated crop production statistics data for 2020 version 1.0.0. Harvard Dataverse, V1. https://doi.org/10.7910/DVN/SWPENT.

IPCC, 2023. Summary for policymakers. In: climate change 2023: synthesis report. In: Core Writing Team, Lee, H., Romero, J. (Eds.), Contribution of working groups I, II and III to the sixth assessment report of the intergovernmental panel on climate change. IPCC, Geneva, Switzerland, pp. 1–34. https://doi.org/10.59327/IPCC/AR6-9789291691647.001.

Jägermeyr, J., Müller, C., Ruane, A.C., Elliott, J., Balkovic, J., Castillo, O., Faye, B., Foster, I., Folberth, C., Franke, J.A., Fuchs, K., 2021. Climate impacts on global agriculture emerge earlier in new generation of climate and crop models. Nat. Food 2 (11), 873–885.

Jeong, J.H., Resop, J.P., Mueller, N.D., Fleisher, D.H., Yun, K., Butler, E.E., Timlin, D.J., Shim, K.M., Gerber, J.S., Reddy, V.R., Kim, S.H., 2016. Random forests for global and regional crop yield predictions. PLoS One 11 (6), e0156571.

Jha, P.K., Beebe, S., Alvarez-Toro, P., Mukankusi, C., Ramirez-Villegas, J., 2023. Characterizing patterns of seasonal drought stress for use in common bean breeding in East Africa under present and future climates. Agric. For. Meteorol. 342, 109735.

Kaaya, A.N., Warren, H.L., Kyamanywa, S., Kyamuhangire, W., 2005. The effect of delayed harvest on moisture content, insect damage, moulds and aflatoxin contamination of maize in Mayuge district of Uganda. J. Sci. Food Agric. 85 (15), 2595–2599.

Kim, Y.U., Webber, H., Adiku, S.G., Júnior, R.D.S.N., Deswarte, J.C., Asseng, S., Ewert, F., 2024. Mechanisms and modelling approaches for excessive rainfall stress on cereals: waterlogging, submergence, lodging, pests and diseases. Agric. For. Meteorol. 344, 109819.

Kumari, M., Chakraborty, A., Chakravarathi, V., Pandey, V., Roy, P.S., 2024. Impact of climate and weather extremes on soybean and wheat yield using machine learning approach. Stoch. Env. Res. Risk A. 38 (9), 3461–3479.

Kurukulasuriya, P., Mendelsohn, R., Hassan, R., Benhin, J., Deressa, T., Diop, M., Eid, H. M., Fosu, K.Y., Gbetibouo, G., Jain, S., Mahamadou, A., 2006. Will African agriculture survive climate change? World Bank Econ. Rev. 20 (3), 367–388.

Leenaars, J.G., Claessens, L., Heuvelink, G.B., Hengl, T., González, M.R., van Bussel, L.G., Guilpart, N., Yang, H., Cassman, K.G., 2018. Mapping rootable depth and root zone plant-available water holding capacity of the soil of sub-Saharan Africa. Geoderma 324, 18–36.

Li, L., Zhang, Y., Wang, B., Feng, P., He, Q., Shi, Y., Liu, K., Harrison, M.T., Li Liu, D., Yao, N., Li, Y., 2023. Integrating machine learning and environmental variables to constrain uncertainty in crop yield change projections under climate change. Eur. J. Agron. 149, 126917.

Lischeid, G., Webber, H., Sommer, M., Nendel, C., Ewert, F., 2022. Machine learning in crop yield modelling: A powerful tool, but no surrogate for science. Agric. For. Meteorol. 312, 108698.

Mertz, O., Halsnæs, K., Olesen, J.E., Rasmussen, K., 2009. Adaptation to climate change in developing countries. Environ. Manag. 43, 743–752.

Meyer, H., Pebesma, E., 2022. Machine learning-based global maps of ecological variables and the challenge of assessing them. Nat. Commun. 13 (1), 2208.

Navarro-Racines, C., Tarapues, J., Thornton, P., Jarvis, A., Ramirez-Villegas, J., 2020. High-resolution and bias-corrected CMIP5 projections for climate change impact assessments. Sci. Data 7 (1), 7.

Ngetich, K.F., Mucheru-Muna, M., Mugwe, J.N., Shisanya, C.A., Diels, J., Mugendi, D.N., 2014. Length of growing season, rainfall temporal distribution, onset and cessation dates in the Kenyan highlands. Agric. For. Meteorol. 188, 24–32.

Obarein, O.A., Amanambu, A.C., 2019. Rainfall timing: variation, characteristics, coherence, and interrelationships in Nigeria. Theor. Appl. Climatol. 137, 2607–2621.

Rattalino Edreira, J.I., Andrade, J.F., Cassman, K.G., van Ittersum, M.K., van Loon, M.P., Grassini, P., 2021. Spatial frameworks for robust estimation of yield gaps. Nat. Food 2 (10), 773–779.
Riedesel, L., Möller, M., Horney, P., Golla, B., Piepho, H.P., Kautz, T., Feike, T., 2023. Timing and intensity of heat and drought stress determine wheat yield losses in Germany. PLoS One 18 (7), e0288202.
Rizza, F., Badeck, F.W., Cattivelli, L., Lidestri, O., Di Fonzo, N., Stanca, A.M., 2004. Use of a water stress index to identify barley genotypes adapted to rainfed and irrigated conditions. Crop Sci. 44 (6), 2127–2137.
Roberts, M.J., Braun, N.O., Sinclair, T.R., Lobell, D.B., Schlenker, W., 2017. Comparing and combining process-based crop models and statistical models with some implications for climate change. Environ. Res. Lett. 12 (9), 095010.
Rosenstock, T.S., Steward, P.R., Shuck, J., Richards, M., Poultouchidou, A., Ombewa, B. V.A., Mumo, E.M., Manda, L., Madalinska, A., Kamau, H., Kagwiria, D., Kamau, H., Madalinska, A., Manda, L., Mumo, E.M., Ombewa, B.V.A., Poultouchidou, A., Richards, M., Shuck, J., Ström, H., 2024. Evidence for Resilient Agriculture Dataset, v1, p. 0.1. https://doi.org/10.7910/DVN/C3YBNN.
Rosenzweig, C., Elliott, J., Deryng, D., Ruane, A.C., Müller, C., Arneth, A., Boote, K.J., Folberth, C., Glotter, M., Khabarov, N., Neumann, K., 2014. Assessing agricultural risks of climate change in the 21st century in a global gridded crop model intercomparison. Proc. Natl. Acad. Sci. 111 (9), 3268–3273.
Rötter, R.P., Appiah, M., Fichtler, E., Kersebaum, K.C., Trnka, M., Hoffmann, M.P., 2018. Linking modelling and experimentation to better capture crop impacts of agroclimatic extremes—A review. Field Crop Res. 221, 142–156.
Sánchez, P.A., 2010. Tripling crop yields in tropical Africa. Nat. Geosci. 3 (5), 299–300.
Shahhosseini, M., Hu, G., Huber, I., Archontoulis, S.V., 2021. Coupling machine learning and crop modeling improves crop yield prediction in the US Corn Belt. Sci. Rep. 11 (1), 1606.
Stuch, B., Alcamo, J., Schaldach, R., 2021. Projected climate change impacts on mean and year-to-year variability of yield of key smallholder crops in sub-Saharan Africa. Clim. Dev. 13 (3), 268–282.
Tao, F., Rötter, R.P., Palosuo, T., Gregorio Hernández Díaz-Ambrona, C., Mínguez, M.I., Semenov, M.A., Kersebaum, K.C., Nendel, C., Specka, X., Hoffmann, H., Ewert, F., 2018. Contribution of crop model structure, parameters and climate projections to uncertainty in climate change impact assessments. Glob. Chang. Biol. 24 (3), 1291–1307.
Ten Berge, H.F., Hijbeek, R., Van Loon, M.P., Rurinda, J., Tesfaye, K., Zingore, S., Craufurd, P., van Heerwaarden, J., Brentrup, F., Schröder, J.J., Boogaard, H.L., 2019. Maize crop nutrient input requirements for food security in sub-Saharan Africa. Glob. Food Sec. 23, 9–21.
van Bussel, L.G., Grassini, P., Van Wart, J., Wolf, J., Claessens, L., Yang, H., Boogaard, H., de Groot, H., Saito, K., Cassman, K.G., van Ittersum, M.K., 2015. From field to atlas: upscaling of location-specific yield gap estimates. Field Crop Res. 177, 98–108.
Van Ittersum, M.K., Van Bussel, L.G., Wolf, J., Grassini, P., Van Wart, J., Guilpart, N., Claessens, L., De Groot, H., Wiebe, K., Mason-D'Croz, D., Yang, H., 2016. Can sub-Saharan Africa feed itself? Proc. Natl. Acad. Sci. 113 (52), 14964–14969.
Van Klompenburg, T., Kassahun, A., Catal, C., 2020. Crop yield prediction using machine learning: A systematic literature review. Comput. Electron. Agric. 177, 105709.
Van Loon, M.P., Deng, N., Grassini, P., Edreira, J.I.R., Wolde-Meskel, E., Baijukya, F., Marrou, H., van Ittersum, M.K., 2018. Prospect for increasing grain legume crop production in East Africa. Eur. J. Agron. 101, 140–148.
Van Oort, P.A.J., 2018. Mapping abiotic stresses for rice in Africa: drought, cold, iron toxicity, salinity and sodicity. Field Crop Res. 219, 55–75.
Van Wart, J., van Bussel, L.G., Wolf, J., Licker, R., Grassini, P., Nelson, A., Boogaard, H., Gerber, J., Mueller, N.D., Claessens, L., van Ittersum, M.K., 2013. Use of agro-climatic zones to upscale simulated crop yield potential. Field Crop Res. 143, 44–55.
Wolf, J., Ouattara, K., Supit, I., 2015. Sowing rules for estimating rainfed yield potential of sorghum and maize in Burkina Faso. Agric. For. Meteorol. 214, 208–218.
Zabel, F., Müller, C., Elliott, J., Minoli, S., Jägermeyr, J., Schneider, J.M., Franke, J.A., Moyer, E., Dury, M., Francois, L., Folberth, C., 2021. Large potential for crop production adaptation depends on available future varieties. Glob. Chang. Biol. 27 (16), 3870–3882.
Zhao, C., Liu, B., Piao, S., Wang, X., Lobell, D.B., Huang, Y., Huang, M., Yao, Y., Bassu, S., Ciais, P., Durand, J.L., 2017. Temperature increase reduces global yields of major crops in four independent estimates. Proc. Natl. Acad. Sci. 114 (35), 9326–9331.
Zhu, P., Abramoff, R., Makowski, D., Ciais, P., 2021. Uncovering the past and future climate drivers of wheat yield shocks in Europe with machine learning. Earth's Future 9 (5) p.e2020EF001815.
Zimmermann, A., Webber, H., Zhao, G., Ewert, F., Kros, J., Wolf, J., Britz, W., de Vries, W., 2017. Climate change impacts on crop yields, land use and environment in response to crop sowing dates and thermal time requirements. Agric. Syst. 157, 81–92.